HIGH TEMPERATURE DURABILITY OF METALS FOR USE IN A PARTICLE HEATING RECEIVER FOR CONCENTRATED SOLAR POWER

A Thesis
Presented to
The Academic Faculty

by

Ryan C. Knott

In Partial Fulfillment
Of the Requirements for the Degree
Master of Science in the
George W. Woodruff School of Mechanical Engineering

Georgia Institute of Technology

December 2014

HIGH TEMPERATURE DURABILITY OF METALS FOR USE IN A PARTICLE HEATING RECEIVER FOR CONCENTRATED SOLAR POWER

Approved by:

Dr. Sheldon M. Jeter, Advisor
George W. Woodruff School of Mechanical Engineering
Georgia Institute of Technology

Dr. Said I. Abdel-Khalik
George W. Woodruff School of Mechanical Engineering
Georgia Institute of Technology

Dr. Peter G. Loutzenhiser
George W. Woodruff School of Mechanical Engineering
Georgia Institute of Technology

Date Approved: November 10, 2014

ACKNOWLEDGEMENTS

I would like to thank everyone who has helped and supported me with this thesis. There are many people who have given their time and energy to make it possible.

Firstly, I would like to thank my advisor, Dr. Sheldon Jeter. His research and professional insight has been a great benefit to my education and my growth as an engineer. I would also like to thank Dr. Said Abdel-Khalik for his expertise and guidance. Another thank you is given to Dr. Peter Loutzenhiser for being a committee member and a research collaborator.

Secondly, I greatly appreciate the support of my coworkers Dennis, Matt, Clayton, Jonathan, Ahmad, and Kenzo; and fellow classmates Robby, Alex, and Maggie.

Lastly, I thank my family and friends who are supporting me even across the country, especially Dad, Mom, Adam, and Jennifer. Their encouragement has helped me continue my education, and I am grateful beyond words.

TABLE OF CONTENTS

LIST OF TABLES

LIST OF FIGURES

LIST OF SYMBOLS

ΔW	Mass Loss
ρ	Density
S	Surface area
v	Wear or Oxidation Speed
Δt	Test Time
k	Weight Gain per Oxidized Volume Coefficient

LIST OF ABBREVIATIONS

CSP	Concentrated Solar Power
HTF	Heat Transfer Fluid
HTM	Heat Transfer Medium
PHR	Particle Heating Receiver
SiC	Silicon Carbide
SS316	316 Stainless Steel
TES	Thermal Energy Storage

SUMMARY

An experimental investigation is presented on a novel High Temperature Falling Particle Receiver for Concentrated Solar Power (CSP) to quantify the extent of erosion of the receiver structural materials by the flowing particulate matter. The current receiver design uses a series of metal wire mesh screens to slow down the particulate flow through the receiver in order to increase their residence time thereby achieving the desired temperature rise within the receiver without the need for particulate recirculation. The solid particulates are gravity fed through the receiver where they absorb the incident thermal energy before flowing to a high temperature storage bin upstream of a heat exchanger where the heat stored in the particulate material is transferred to the working fluid for the power cycle. To assess the effective life of the receiver, this experimental investigation is undertaken. This thesis includes the development of an apparatus to test wire meshes under high temperature and particle abrasion conditions, and the presentation and analysis of these results.

The metals considered for a Particle Heating Receiver (PHR) include stainless steel 316, nickel-chromium (Chromel C), and non-sag tungsten. Each metal shows a trend of increasing mass as the number of cycles increases. This is believed to be due to oxidation. The temperature of the experiment is sufficiently high to encourage the rapid formation of oxidized materials within each sample. The combination of impact by the particulate and oxidation are acting on the surface of the metals. However, the oxidation appears to be a greater contributing factor to the mass change of the samples. When tested, the stainless steel 316, non-sag tungsten, and nickel-chromium alloys showed an increase in mass. This is consistent with oxidation. As the number of cycles increases, the surface area becomes more fully oxidized. Future work to be done for

PHR materials should include determining the length of meshes to be used in the PHR determined by the thickness of the falling particle curtain, the overall efficiency and convective losses in such a PHR, and methods to mix the particles in the PHR from front to back and vice versa to ensure a uniform particle temperature.

CHAPTER 1

INTRODUCTION

Concentrated Solar Power (CSP) is a method of concentrating solar radiation for useful work or processes, illustrated in Figure 1.1. The solar radiation is focused to the desired area in a receiver and the heat is absorbed by a medium being circulated through the focused light called a Heat Transfer Fluid (HTF). The HTF is passed through the receiver and then through a heat exchanger. After the heat is exchanged to a working fluid such as CO_2, the working fluid is then used to drive a power generation cycle. Then the HTF is either stored in a large reservoir or recirculated through the receiver as necessary. These fluids are most typically steam or molten salts. Both media require extensive recirculation systems which add cost to the overall system. Additionally, typical molten salts are corrosive to steel pipes, and solidify if the temperature drops below the salts' melting point. Heat must be applied to the pipes to liquefy the salts and restart the power plant. Solid particulates such as silica sand or alumina grains are materials being investigated for use in a CSP plant to replace steam and molten salts as an HTF. These solid particulates are cost effective, commercially available, and provide inherent Thermal Energy Storage (TES) advantages. Current investigations into solid particulates as an HTF have identified several challenges including recirculation from heat exchanger back to the receiver, selection of a type of particulate to use, and increasing the heat transfer efficiency of the particulate in the focused light. To increase the efficiency, a receiver is designed to increase the residence time of particulate in the focused light thus reducing the need for recirculation to achieve a desired temperature rise. This thesis is concerned with the receiver designed for use with solid particulates.

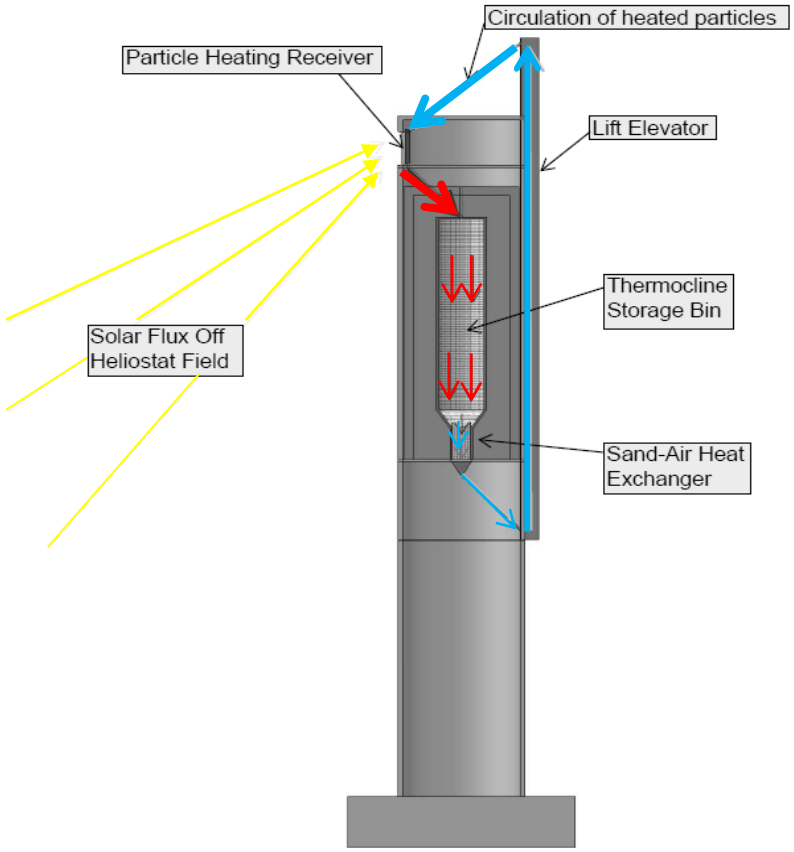

Figure 1.1 CSP System with Solid Particulate as HTF

Several receiver designs have been explored including porous silicon carbide blocks, free falling curtains, and discrete porous structures such as wire meshes. The discrete porous structures have the most promise since they can be constructed in many different ways to control the mass flow through the receiver. Current designs of the structures are in the shape of chevrons, as shown in Figure 1.2.

Figure 1.2 Discrete Porous Structure Wire Mesh Chevron Configuration

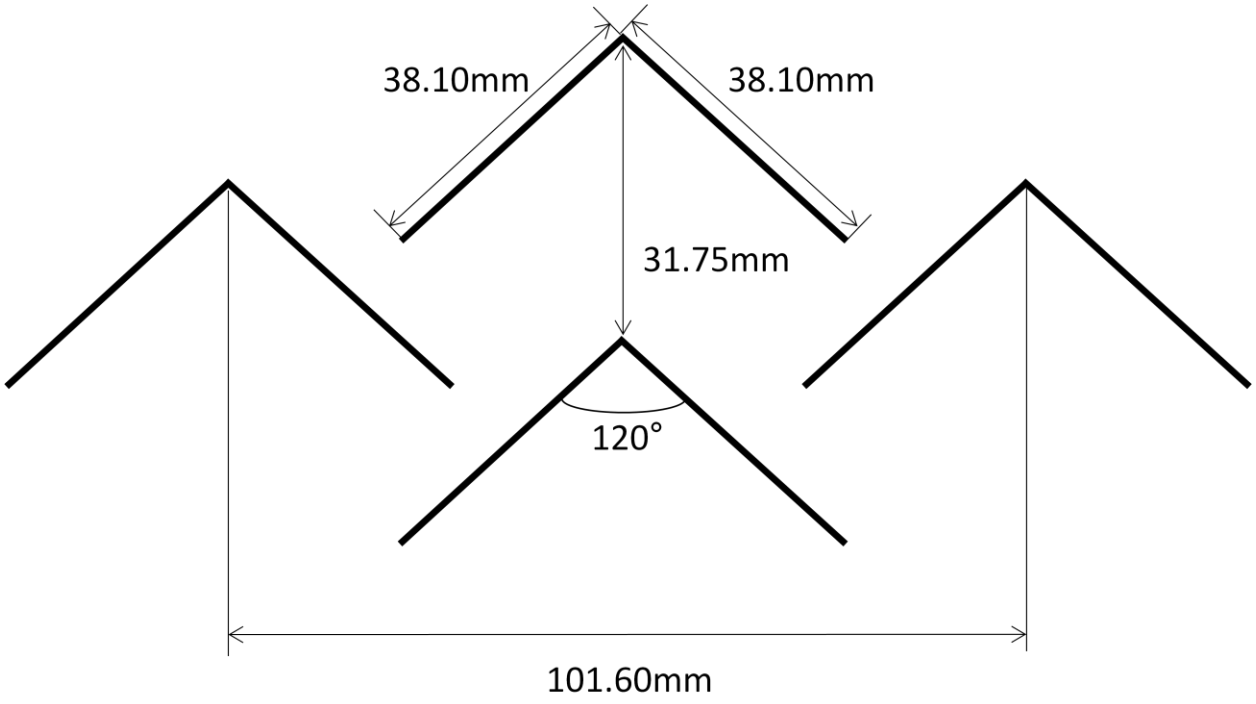

Figure 1.3 Diagram of Discrete Porous Structure Chevron Pattern

Each chevron side has a length of 38.1 mm and an angle of 120° between the two sides. A diagram of the chevron design is shown in Figure 1.3. The necessary chevron depth into the

receiver is currently being investigated. Wire mesh chevrons at different elevations in the receiver may experience different particulate mass fluxes as the particulate flow area expands. Additionally, the wires which make up the chevron will have a specified spacing and thickness which are dependent upon the size of the particles and the desired mass flow.

When combined with many other wire mesh chevrons, the particles which are being fed by gravity through the receiver must impact the wire meshes thus decreasing their velocities. Over a large area and with changes to the open areas of the meshes themselves, the mass flow of the particulate can be controlled and the residence time in the concentrated sunlight increased. This increase in the residence time will increase the particles' temperature. A higher temperature leads to a higher cycle efficiency. A fully built receiver is shown in Figure 1.4.

Since the metal meshes are being impacted by solid particles and the temperature of the particles is expected to be in excess of 800°C, concerns arose over what materials would be most ideal for the wire meshes. The experiment conducted and discussed in this thesis addresses those concerns.

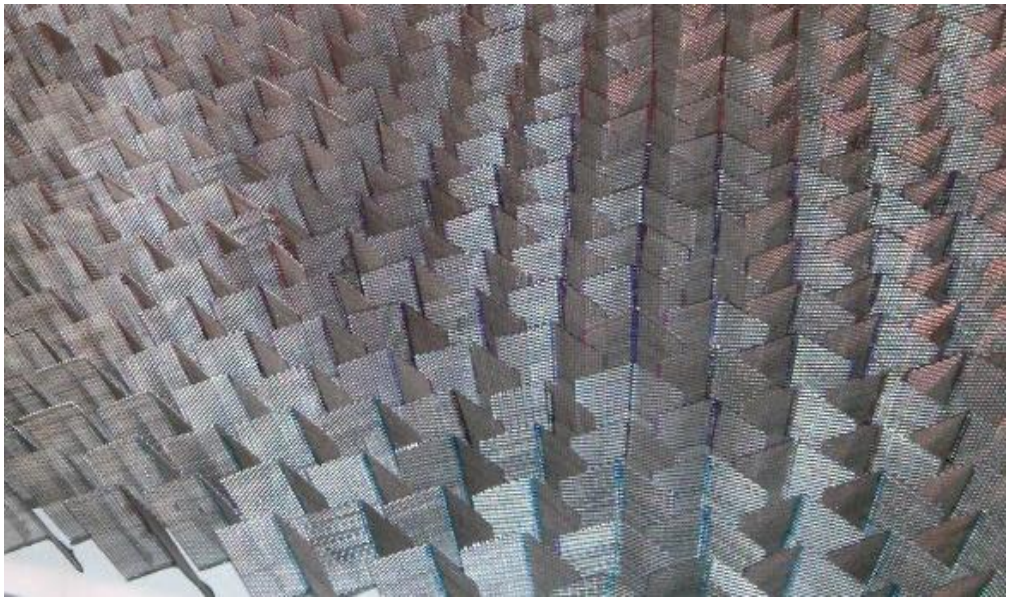

Figure 1.4 Complete Receiver with Metal Wire Mesh Chevrons

CHAPTER 2

LITERATURE REVIEW

Concentrated Solar Power with Solid Particulates

Using solid particulates as a heat transfer and thermal energy storage medium in CSP systems is a concept which has been explored since the early 1980s. A feasibility study by Babcock and Wilcox for Sandia National Laboratories recommended in 1981 a moving bed thermal energy storage system with a refractory material as the HTM for an eventual full scale tower system [1]. Further studies analyzed the economics and technical challenges for CSP systems using solid particulates. Martín and Vitko [2] considered design concepts and also listed some of the future research which had to be done, including the design of the receiver, the design of the lift system to recirculate particles, and qualities for an ideal particulate candidate. However, this was preliminary research, and a technical feasibility paper was published by Hruby [3]. Hruby compiled technical evaluations about the various components of CSP with solid particulates such as a free-falling curtain receiver, the material of the solid particulates, how to evaluate the performance and cost of the material, and particle lift systems and heat exchangers [4-8]. The free-falling curtain receiver has received the most attention, but several other types of receivers have been suggested, including those which can increase the maximum cycle temperature of the particles. This increase in temperature is a means to increase the overall efficiency of CSP.

Particle Heating Receivers

In her recommendations, Hruby suggested that a technique of maintaining "a high volume fraction particle flow" was to reduce the amount of spread that particles experienced as a result of acceleration when falling. She suggests that "one way of achieving less particle spread may be to insert ceramic objects supported on the back cavity wall into the flow. The particles would decelerate when making contact with these inserts and therefore less spread between the particles in the vertical direction would occur." [3] However, due to limited computational power, the design was only recommended as a way to increase the efficiency and not analyzed. Figure 2.1 shows Hruby's concept.

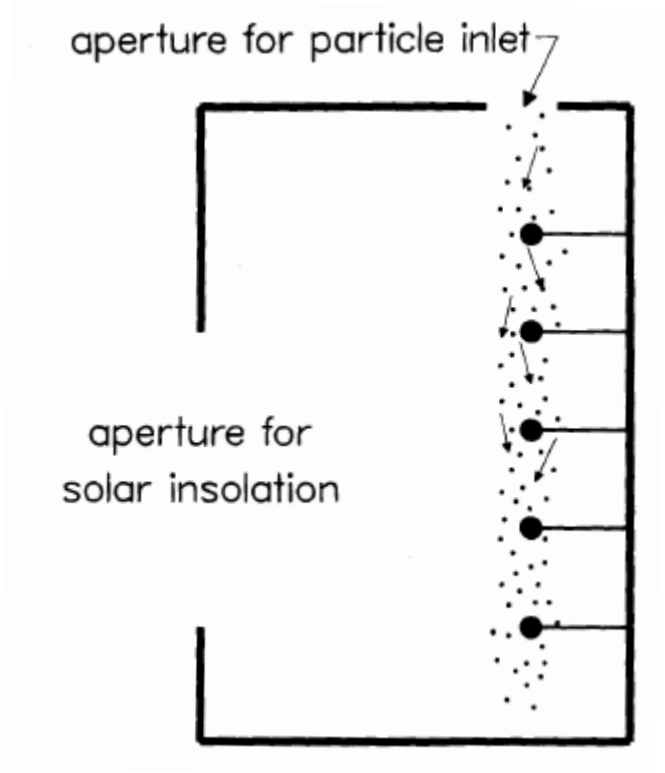

Figure 2.1 Particle Heating Receiver Design to Prevent Thinning Falling Curtain, Proposed by Hruby [3]

Although solid particles as an HTM for CSP were explored in the 1980s, the design for CSP moved in favor of using nitrate salts and steam. Ho and Iverson [9] reviewed the work which has been done on high-temperature central receivers for CSP and noted that "Although a number of analytical and laboratory studies have been performed since its inception in the 1980s… those preliminary tests, which did not optimize the configuration of the receiver aperture, only achieved 50% thermal efficiency, and the increase in particle temperature was ~250℃ from ambient conditions." One of the methods they recommended for increasing the thermal efficiency is from Hruby's [3] technical summary, which is to "increase the residence time of the particles within the concentrated beam." Roesle et al. [10] explored the radiative properties of particle suspensions for CSP applications, which held the particles fixed in an epoxy resin. In this thesis, the PHR is designed with falling particles. Two types of receivers have been explored to increase the residence time of the particles: a porous structure and a discrete structure.

Golob et al. [11] have examined the porous structure style receiver. The receiver itself is a silicon carbide foam formed when a sponge-like foam made of plastics is dipped in a SiC solution. The plastic is eliminated from the inside structure and the SiC is left. Figure 2.2 shows an example of the porous SiC foam. The SiC receiver retains pores through which the solid particulates are allowed to flow and their residence time is increased due to the restrictive size of those pores. This type of receiver has shown promise, but there are difficulties in achieving the desired mass flow of solid particulate through the receiver. In the same paper the discrete structure PHR is also discussed. Instead of being one unit, the filaments and branches that make up the SiC foam consist of meshes which can be laid in any configuration and with any mesh size, which is to say the spacing between wire filaments. This method is especially useful when

the design needs to be changed quickly. It is also less expensive than the SiC foam, and can be made of many different materials. Figure 2.3 shows a discrete structure wire mesh.

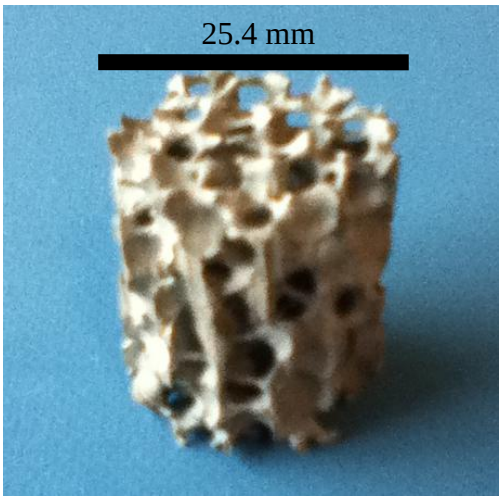

Figure 2.2 Porous SiC Structure (25.4 mm Diam., 25.4 mm Height) for a PHR

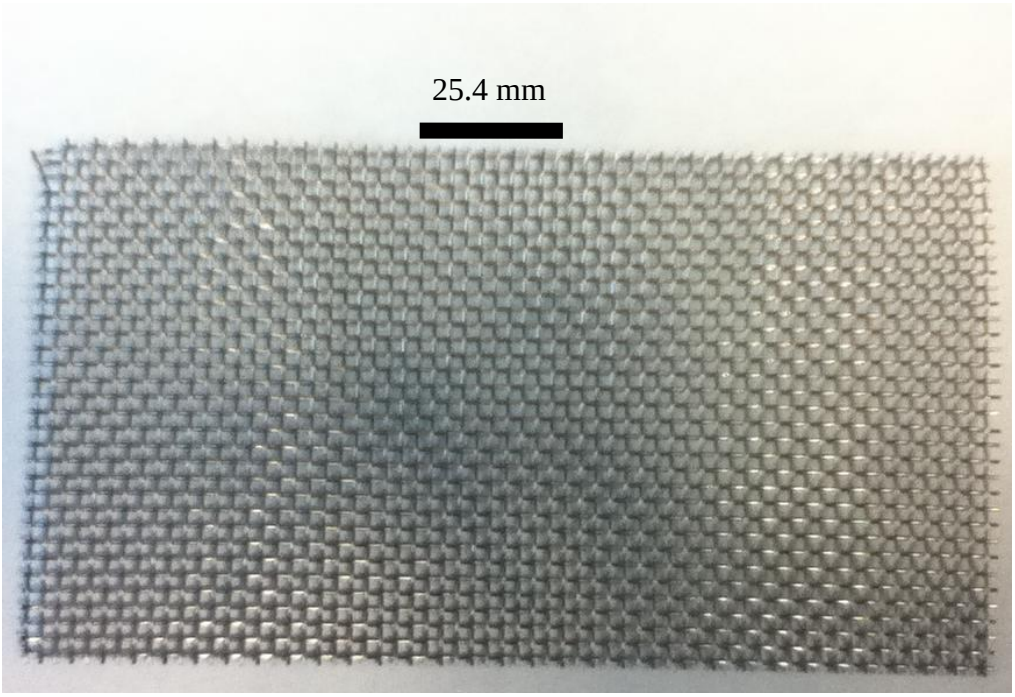

Figure 2.3 Discrete Structure Wire Mesh (U.S. 10 Mesh)

Durability of Discrete Structures in a Particle Heating Receiver

A concern which existed about discrete structures was their durability. A receiver which fails can release bits of the discrete structures into the particulate. Fouling of the particulate can cause a decline in the heat exchanger effectiveness, especially if fins that are installed in the heat exchanger catch the discrete structure filaments. The decrease in effectiveness decreases the thermal efficiency of the system. Another issue which could arise would be overheating of the back wall if the receiver is tall enough for particles to begin separating in a free-falling curtain receiver. If the discrete structures failed, the particles would no longer be densely packed vertically. The back of the receiver would experience a large amount of solar radiation, possibly more than was intended. The receiver cavity would fail as well. To measure the durability of metals under conditions expected in the PHR, the materials are weighed before and after the expected PHR conditions.

In order to prevent failures of the PHR from happening, the discrete wire mesh structures must be able to withstand high-temperature particle impacts. There have been previous studies on the effects of high-temperature silica sand particles abrading against metal samples. Liu et al. [12] designed a rotating abrasion tester. A rotating arm is inserted into a sand bed at 923 K and the arm rotates at 200 rpm, which translates to a speed of 1.36 m/s. The metal test specimens face the direction of the rotating arm but are fixed at 45° from the tangent of the circular motion of the rotating arm. Each sample is a solid block 100 mm x 100 mm x 25 mm of hypereutectic high Cr cast iron which was cast in a sand mold. To measure the wear rate, Lieu et al. used Equation 1:

$$\Delta W = \rho S_w v_w \Delta t - k S_o v_o \Delta t \quad (1)$$

where ΔW is the mass loss, ρ is the density, S is the surface area, v is the wear or oxidation speed, Δt is the test time, and k is the weight gain per oxidized volume coefficient. A "w" or "o" represents wear and oxidation, respectively. Rearranged, Equation 1 becomes a wear rate as shown in Equation 2:

$$v_w = \frac{\Delta W + k S_o v_o \Delta t}{S_w \rho \Delta t} \tag{2}$$

Liu et al. require that the oxidation rate be known or tested experimentally. This experiment has harsher conditions on the metal samples than will be experienced in a PHR. The speed experienced by the metal sample was 1.36m/s through a packed bed of quartz sand. At this speed and temperature, Liu et al. report that their samples experienced greater weight loss than weight gain due to oxidation. According to studies performed by Nguyen et al. [12] the maximum speed that the particles should experience in a discrete porous structure at the current design considerations is on the order of 0.35 m/s. The PHR will experience only 7% of the kinetic energy with which Liu et al. tested. Additionally, the particles used by Liu et al. have a mean diameter of 1 mm, which is three times the diameter expected in a CSP system with a PHR. Misra et al. [13] notes that a metal such as Tungsten was found to have "higher wear resistance from smaller abrasive particles… whereas for larger particles it has lower than the expected value of wear resistance." The experimental results from Liu et al. are not suitable for predicting wear for a discrete porous PHR, but the wear rates presented in Equation 2 are useful in conditions of oxidation and wear. Instead, an apparatus which can accurately simulate prototypical PHR conditions is devised in Chapter 3.

CHAPTER 3

EXPERIMENTAL APPARATUS

To determine the change in mass of a wire mesh due to both abrasion by particles and elevated temperatures, an apparatus was designed to pass particles through mesh samples while operating at high temperatures. A 316 stainless steel (SS316) pipe 18 inches long (0.45 m) and 1 inch in inner diameter (25.4 mm) is selected. A fixed inventory of particles is poured into the pipe with an endcap screwed on to the pipe to catch the particles at the bottom of the pipe. Fixed to the endcap is a 500W cartridge heater with an internal K-type thermocouple embedded inside the cartridge. The mesh samples to be tested are installed between two expansion rings which are fixed in place with set screws tightened in two tapped holes in the SS316 pipe. Then another endcap with a cartridge heater is installed on the free end of the pipe. The pipe rests in the center of four 1 inch (25.4 mm) Fibrafrax Duraboard insulation sheets and the endcaps are covered by insulation as well with the electrical leads and thermocouples of the heaters extending out of the insulation. The described apparatus is shown in Figure 3.1 and Figure 3.2.

The ends of the pipe are threaded. Two through-holes are tapped in the steel pipe, each 1.25 inches (31.75 mm) from the center of the pipe such that the two holes are symmetric about the center. Two expansion rings are machined from SS316 and a groove is cut in them such that the rings are no longer continuous in a radial direction, but are now flexible. The expansion rings prevent the particulate from experiencing plug flow, which is particulate that moves as a single mass downward rather than flowing.

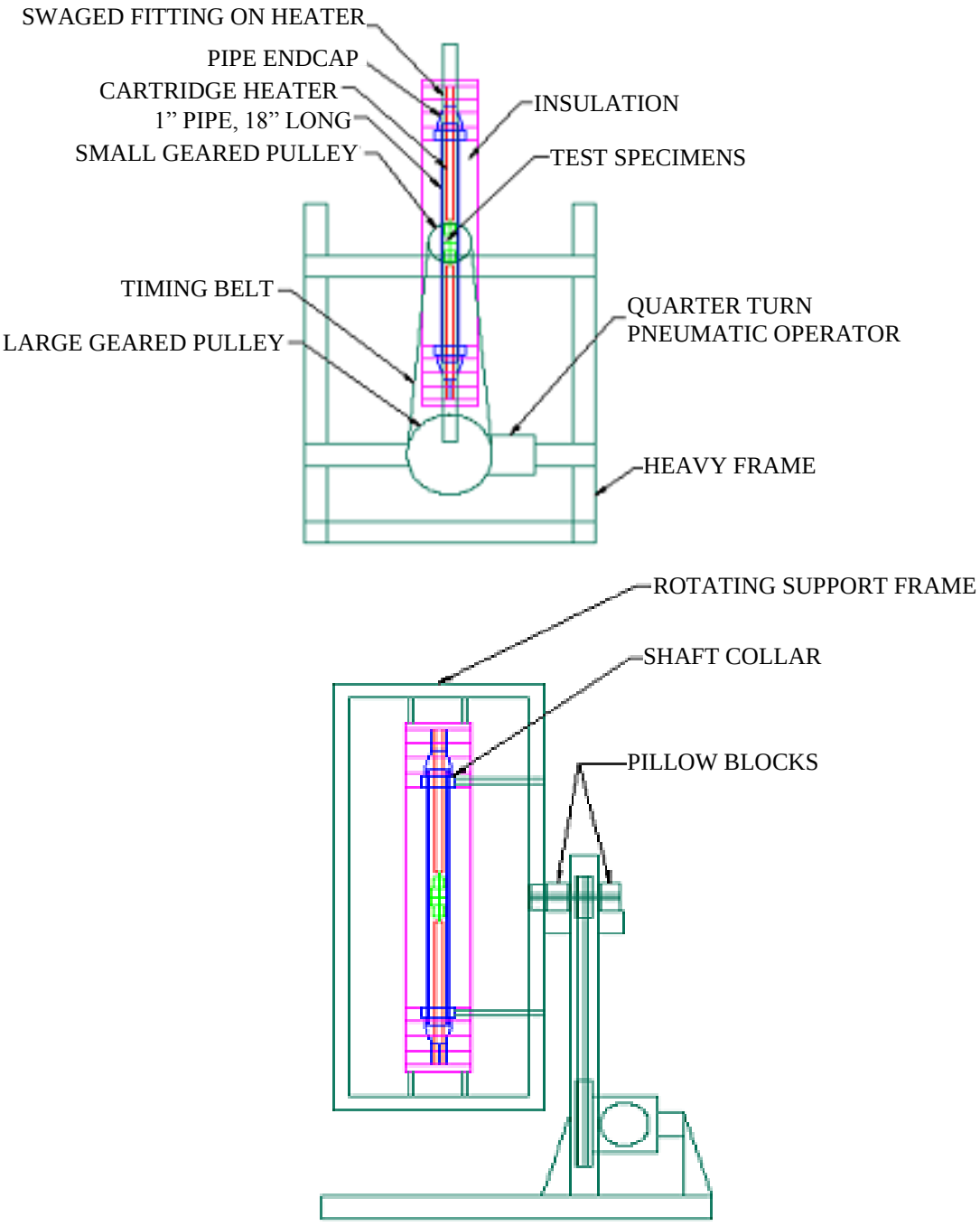

Figure 3.1 Schematic of Hourglass Apparatus

Front View (Top) and Side View (Bottom)

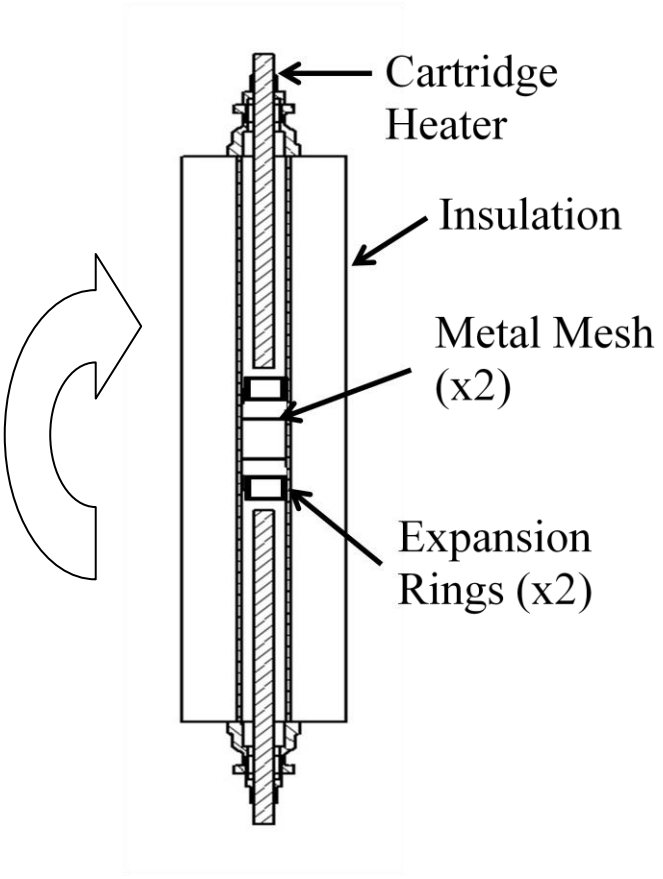

Figure 3.2 Diagram of the Hourglass Apparatus

The cartridge heaters have an Incoloy sheath with magnesium oxide insulation and a K-type thermocouple embedded inside. To hold the heaters in place, a Swagelok fitting is used per heater. The fitting is slid onto the heater and fixed in place by tightening the nut on the Swagelok fitting. The nut is tightened 0.5 inches (12.7 mm) from the wired end of the cartridge heater with the threaded end facing the non-wired end of the cartridge heater. Each heater is fixed to a Swagelok fitting. The threaded end of the fittings are screwed into a pipe endcaps which are bell-shaped. Figure 3.3 shows the cartridge heater assembly.

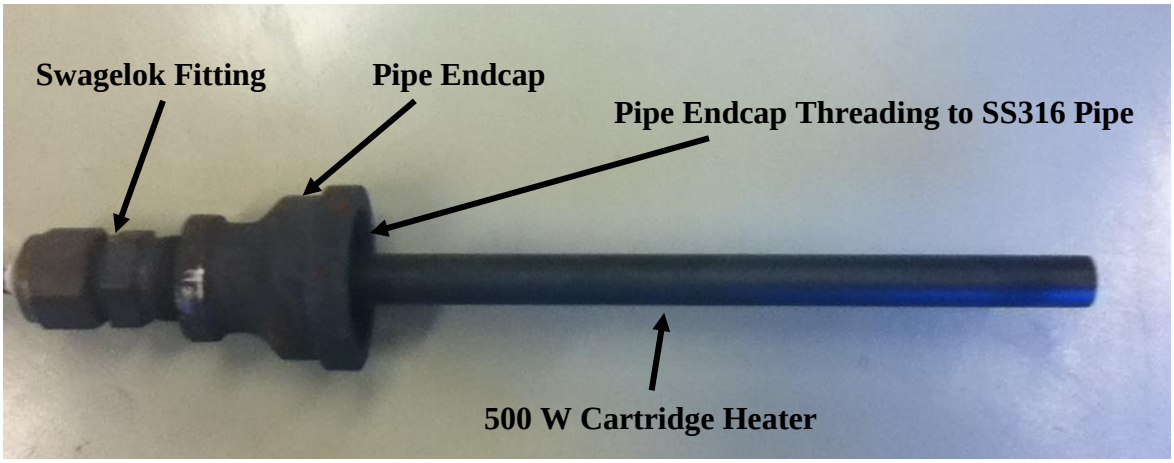

Figure 3.3 Cartridge Heater Assembly

The narrow end of the endcaps is screwed into the Swagelok fittings while the large end of the endcaps is threaded to match the ends of the SS316 pipe. These endcaps keep the particles inside the apparatus. To ensure that the embedded thermocouples are reading properly, three K-type thermocouples are attached using metal pipe hoops which are crimped into place, holding the thermocouples against the pipe at uniform intervals. Between each endcap and the insulation, a metal shaft collar with a threaded hole is fixed to the pipe by slipping the collar on the pipe and tightening a threaded rod to press the pipe against the collar. The rods face the same direction and will be used as structural support for the apparatus. To provide electricity for the heating cartridges, a variable AC (variac) power supply is used with a 10 A fuse. The heating cartridges are connected in parallel to each other, as shown in the block diagram in Figure 3.4.

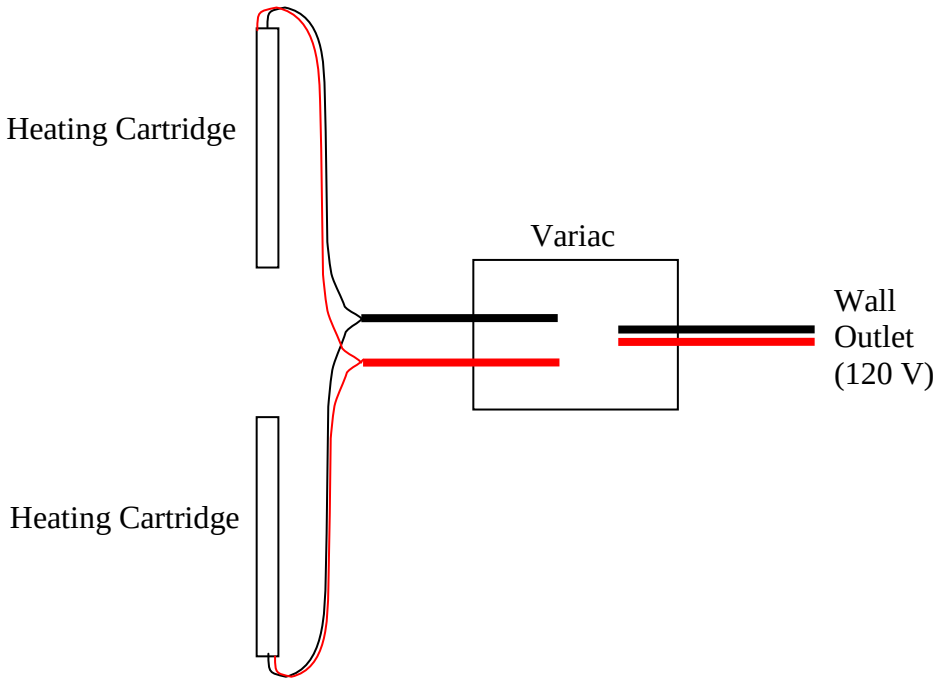

Figure 3.4 Electrical Diagram of Heating Cartridges as Installed in Experiment: in Parallel

Fiberfrax Duraboard is used as insulation around the SS316 pipe. This insulation is sold in 1 inch (38.1 mm) thick sheets. Four of these sheets stacked together form the insulation for the apparatus. The inside of the innermost two sheets is shaved until the SS316 pipe can rest inside the insulation. The same is done for the cartridge heaters and endcaps. Figure 3.5 shows the pipe resting in the Duraboard insulation.

Figure 3.5 SS316 Pipe Sitting in Duraboard Insulation Fitted to Pipe with External K-Type Thermocouples Fixed in Place

Four holes are drilled at the corners of the Duraboard to allow bolts to pass through the entire insulation assembly. When the insulation is pressed together and the bolts fit through the insulation, the assembly resembles Figure 6 shown below.

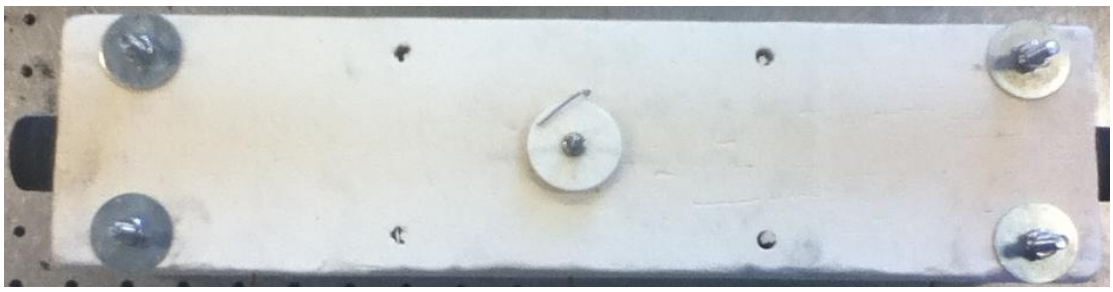

Figure 3.6 Insulation Bolted and Tightened Together Around SS316 Pipe

As shown in Figure 6 there is a hole in the center with a Duraboard plug fixed in place using a staple. The staple and plug can be removed and the surface temperature of the SS316 pipe can be checked using an infrared thermometer.

The assembly is fixed to a rotating metal frame using the threaded rods of the collars between the endcaps and the insulation. The threaded rods are fixed to the metal frame using hex

nuts on either side of the metal frame where the rods pass through. Additionally, on either side of the endcap insulation blocks are two u-shaped brackets. These brackets keep the apparatus rigid relative to the metal frame. The frame is attached to a rotating rod which is passed through two pillow blocks. On the rotating rod is a small-geared pulley. The small-geared pulley is acted on by a timing belt which in turn is acted on by a large-geared pulley. A quarter turn pneumatic actuator periodically rotates the large-geared pulley in specified intervals.

In summary, the apparatus consists of a SS316 pipe with a fixed inventory of particles inside and two mesh samples equally spaced at the midplane of the pipe each between an expansion ring. The ends of the pipe are capped with endcaps screwed onto pipe fittings which secure 500 W cartridge heaters. The assembly is encased in Duraboard insulation and attached to a rotating frame via shaft collars and threaded rods. The threaded rods are bolted to a rotating frame, and the frame is connected to a rod which is allowed to rotate in pillow blocks. The frame and the apparatus rotate as a single piece while the pneumatic actuator is fixed in place turning the gears with the timing belt. The heating cartridges heat the SS316 pipe assembly and the rotations cause the particulate to fall, abrading against the metal mesh samples. With this apparatus the conditions of the discrete structure particle heating receiver can be replicated and the durability of the metal wire mesh structures analyzed.

CHAPTER 4

EXPERIMENTAL PROCEDURE

To measure the change in mass of the metal mesh samples, the apparatus described in Chapter 3 is used. First, a known mass of particles is selected to abrade against the meshes. It should consist of a material that is expected to be used in a PHR in the future. A foundry material called ID50-K is selected. Appendix A shows the material properties of ID50-K. The material is spherical and uniform in composition, size, and shape. To ensure that the particles used in the experiment are indeed uniform in size, a mechanical vibrating sifter is used. A sifter is a series of mesh sieves stacked one upon the other, with the bottommost sieve being completely solid. As the particles are vibrated, they are allowed to rotate and position themselves across the mesh face. Particles which are smaller than the openings of the meshes fall through the mesh and land on the next sieve. Particles which are too big remain trapped on the mesh. This pattern is repeated from a large mesh opening to a small mesh opening for the desired ranges of particle sizes. Appendix B includes more details about the sifter and the process for sifting particles. In this experiment, ID50-K particles which pass through a U.S. 50 mesh sieve (opening size of 0.300 mm) but are stopped on a U.S. 70 mesh sieve (opening size of 0.212 mm). This is to exclude particles which may be too big to pass through the mesh samples in the experiment and also prevent fine particles which may not achieve similar falling velocities as will be experienced in a typical discrete structure PHR. Once the particles are sifted, 150 g of particulate are weighed and ready for use in the experiment.

Next the mesh samples are prepared. A 12 inch by 12 inch sheet (304.8 mm by 304.8 mm) of metal mesh is selected. The wire filaments which make up the mesh are 0.025 inches

(0.635 mm) in diameter and consist of the material to be tested. Two 1 inch (25.4 mm) circles are cut from the sheet using shears. Previously a die cutter had been used but it was found to crush and alter the shape of the wires. Each wire should be cut individually to prevent shape distortion. Once the two circles are cut from the wire mesh sheet, the circles are trimmed to make sure that they will fit properly in the pipe without scraping the inside of the pipe. Figure 4.1shows a sample. Each sample is weighed on an Ohaus Pioneer PA64 Analytical Balance ten times to establish an average mass. The Ohaus balance measures to 0.0001 g.

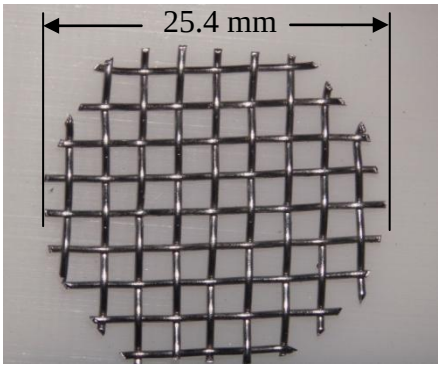

Figure 4.1 SS316 Wire Mesh Sample

Two 1/16 inch (1.59 mm) diameter SS316 rods are cut to a length of 2.5 inches (63.5 mm). These rods are passed through the mesh samples and fixed to the samples using side-mount external retaining rings. The rings fit on either side of the mesh sample and hold the sample at a fixed location on the rods. The spacing of the meshes is 1.25 inches (31.75 mm) and the meshes are symmetric about the center of the rods. Figure 4.2 shows the mesh-rod assembly.

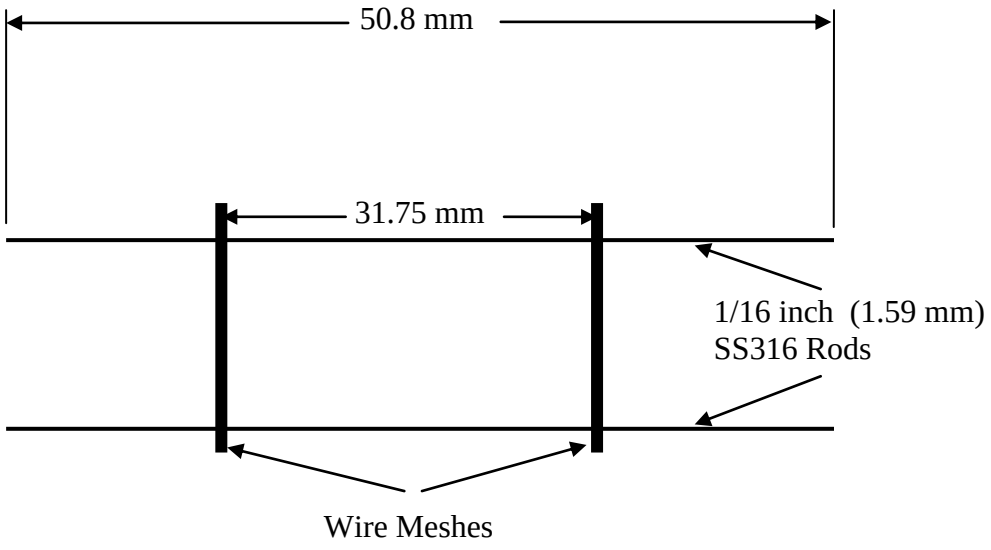

Figure 4.2 Wire Mesh Samples with SS316 Rods

One expansion ring is then moved into place and fixed with a set screw tightened through the SS316 pipe. Then the wire mesh samples which are now fixed in place relative to each other via SS316 rods are inserted into the pipe. The rods rest on the expansion ring. Then the other expansion ring is installed in the same manner as the first. The expansion rings serve two purposes which are allowing the particulate room to decrease in bulk density before reaching the meshes and holding the wire mesh samples in place.

After the wire mesh samples are installed and held in place using the expansion rings, the sifted particulate is poured into the pipe. Then the second and last endcap is screwed onto the pipe and the insulation is slipped on and bolted around the pipe. The insulated pipe is brought to the rotating frame and installed, inserting threaded rods into bolt holes where hex nuts are tightened to make the pipe assembly and the rotating frame fixed relative to each other. The heating cartridges are connected to a variac and the timing on the pneumatic pulley system is set to rotate once every 15 seconds. The rotation is begun and the variac is switched on to 85 V.

Once the heating begins, the temperature is monitored every 30 minutes via the internal K-type thermocouples embedded in the heating cartridges and the external thermocouples installed on the outside surface of the pipe. Adjustments in the voltage applied to the cartridges are made until the desired temperature is achieved. The voltage is noted and the experiment runs for the desired amount of time. Below in Figure 4.3 the hourglass apparatus is installed in the rotating frame and its temperature is 800°C, as evidenced by the glowing red pipe.

Figure 4.3 Hourglass Experiment at 800°C

Once the desired time has been reached, the final temperature is noted and the variac is switched off. The experiment is left to cool. Now cool, the pipe assembly is removed from the rotating frame, the insulation is taken off the pipe, an endcap is unscrewed, and an expansion ring is taken out of the pipe assembly. The mesh samples are taken out of the pipe, the metal rods disconnected from the samples, the mesh samples are dusted using air at a low velocity, and the

meshes are weighed ten times on the same balance used previously. The new mass is recorded. The process is repeated as needed for different materials and different temperatures. This experimental procedure was carried out with the experimental apparatus outlined in Chapter 3, and the results are presented in the next chapter.

CHAPTER 5

RESULTS

The results of the experiments are shown in the tables below for the test specimens. Each cycle is 15 seconds long.

Table 5.1 Stainless Steel 316 Results at 800°C

SS316 Test Run	Duration of Test (Cycles)	Beginning Mass of Mesh (g)	Ending Mass of Mesh (g)	Percent Mass Change
1*	11520	Mesh 1: 0.693	Mesh 1: 0.694	+0.1444%
		Mesh 2: 0.800	Mesh 2: 0.800	0%
2	11520	Mesh 1: 0.6367	Mesh 1: 0.6375	+0.1256%
		Mesh 2: 0.6526	Mesh 2: 0.6533	+0.1073%
3	40320	Mesh 1: 0.6375	Mesh 1: 0.6377	+0.0315%
		Mesh 2: 0.6533	Mesh 2: 0.6534	+0.0153%

*Test run was with another balance which had less precision.

Table 5.2 Nickel-Chromium Results at 800°C

Nickel-Chromium Test Run	Duration of Test (Cycles)	Beginning Mass of Mesh (g)	Ending Mass of Mesh (g)	Percent Mass Change
1	5760	Mesh 1: 0.9768	Mesh 1: 0.9778	+0.1024%
		Mesh 2: 0.8540	Mesh 2: 0.8548	+0.0937%
2	11520	Mesh 1: 0.9778	Mesh 1: 0.9781	+0.0307%
		Mesh 2: 0.8548	Mesh 2: 0.8552	+0.0468%
3	17280	Mesh 1: 0.9781	Mesh 1: 0.9782	+0.0102%
		Mesh 2: 0.8552	Mesh 2: 0.8552	0%
4	23040	Mesh 1: 0.9782	Mesh 1: 0.9783	+0.0102%
		Mesh 2: 0.8552	Mesh 2: 0.8552	0%

Table 5.3 Non-Sag Tungsten Results at 800°C

Non-Sag Tungsten Test Run	Duration of Test (Cycles)	Beginning Mass of Mesh (g)	Ending Mass of Mesh (g)	Percent Mass Change
1	5760	Mesh 1: 1.487	Mesh 1: 1.489	+0.1345%
		Mesh 2: 1.398	Mesh 2: 1.401	+0.2146%
2	11520	Mesh 1: 1.489	Mesh 1: 1.490	+0.0672%
		Mesh 2: 1.401	Mesh 2: 1.402	+0.0714%
3	17280	Mesh 1: 1.490	Mesh 1: 1.491	+0.0671%
		Mesh 2: 1.402	Mesh 2: 1.402	0%
4	23040	Mesh 1: 1.491	Mesh 1: 1.491	0%
		Mesh 2: 1.402	Mesh 2: 1.403	+0.0713%

*Non-sag tungsten is tungsten which has been doped with potassium-aluminum silicate.

CHAPTER 6

DISCUSSION

Hourglass Apparatus

Each metal shows a trend of increasing mass as the number of cycles increases. This is believed to be due to oxidation. The temperature of the experiment is sufficiently high to encourage the rapid formation of oxidized materials within each sample. Figure 6.1 shows a microphotograph of a typical stainless steel 316 sample after oxidation. The combination of impact by the particulate and oxidation are acting on the surface of the stainless steel. The same process occurred on the other metals. However, the oxidation appears to be a greater contributing factor to the mass change of the samples. When tested, the SS316, non-sag tungsten, and nickel-chromium alloys showed an increase in mass. The tungsten alloy sample shows some oxidation as the number of cycles increases. This rate of increase is 1.22 ± 0.30E-7 grams per cycle over the period of testing. However, as evident in Figure 6.4 and Table 5.3, the tungsten alloy's rate of increase is decreasing as the number of cycles passes 15000. This is consistent with oxidation. As the number of cycles increases, the surface area becomes more fully oxidized until saturated. The same is seen for the stainless steel samples.

The experiments have also shown that a nickel-chromium alloy (Chromel C) does not show observable wear as well, similar to the tungsten alloy. Its rate of increase is slower than that of the tungsten. This could be a slower oxidation process or increased rate of wear counteracting the mass increase of the nickel-chromium alloy. The materials of interest for building a discrete porous mesh structure at operational speeds and cycles are durable for use in a

particle heating receiver. To confirm that this experiment does indeed destroy mesh samples made of soft materials, copper was also tested.

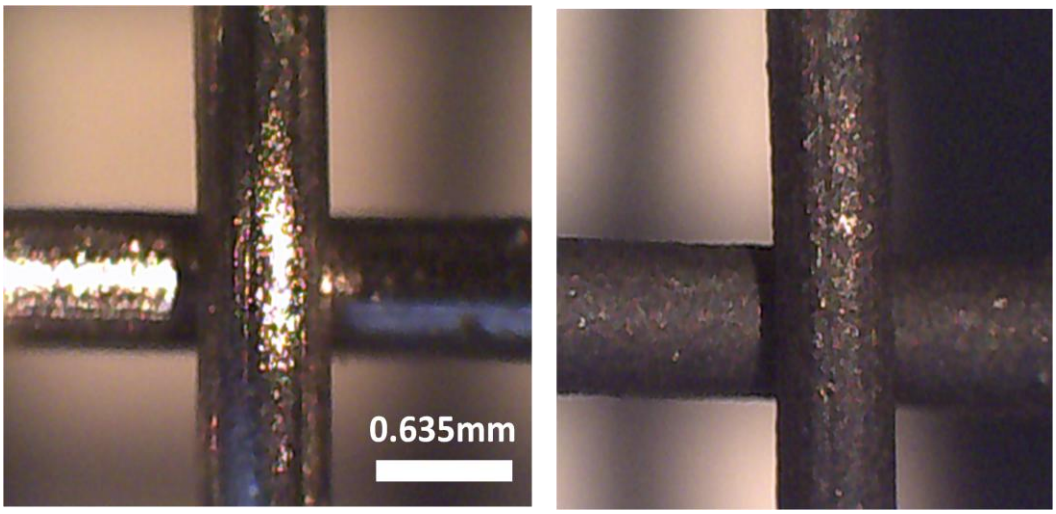

Figure 6.1 Microphotograph of Stainless Steel 316 Untested (Left) and After 5760 Cycles at 800°C with Impacting Alumina (Right)

When a copper mesh was tested as a method to check if a weaker material would fail, the mesh was found to be broken into pieces after the first round of cycles. Copper as a material fails and is not a candidate for a receiver. The resulting mass is not shown, because if a mesh fails, then the material that constituted that mesh is not suitable for a PHR. Figure 6.2 shows the copper mesh before and after testing. The copper mesh shows signs of oxidation and scaling, which is being eroded away. As time progresses, the copper becomes more brittle and material is abraded off by the falling alumina particulate. The copper mesh then fails. Figure 6.3 shows a failed filament.

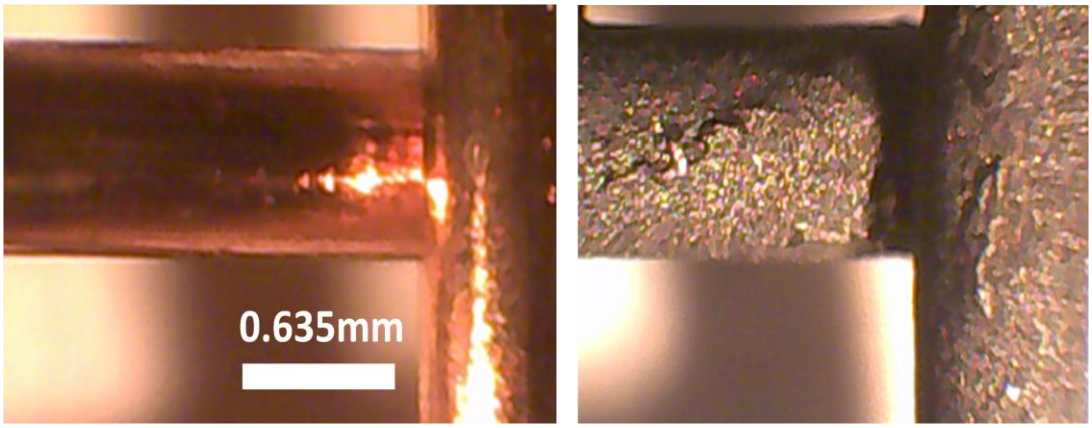

Figure 6.2 Microphotograph of Copper Untested (Left) and After 5760 Cycles at 800°C with Impacting Alumina (Right)

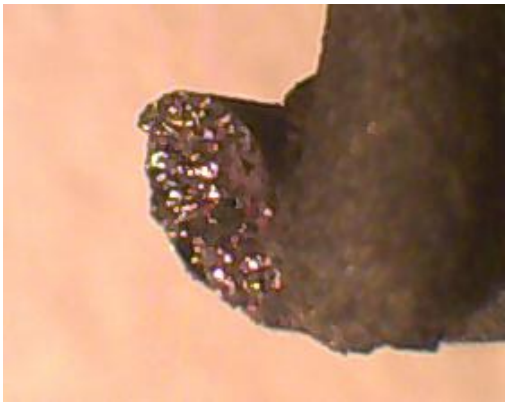

Figure 6.3 Microphotograph of Filament of Tested Copper (Broken)

Summarizing pertinent error analysis, the average uncertainty due to random error (obtained from regression analysis with the tungsten alloy) is 0.00056 grams, and the estimated uncertainty due to possible measurement bias is only 0.0001 grams, due to uncertainty in the precision balance. Consequently the average combined uncertainty is 0.00058 grams. The

average uncertainty is lower for the nickel-chromium alloy because its uncertainty due to data variability is less than that of the tungsten, and the uncertainty due to the measuring instrument i.e. the balance is the same.

The metals that have the most promise for PHR applications are the ones which survive the test and also show no appreciable mass decrease, which is a sign that the material is wearing away. Stainless steel 316, “no-sag” tungsten, and the Chromel C nickel-chromium alloy are metals suitable for a PHR, according to this experiment.

Testing will continue in order to determine the durability of other metals and ceramics considered for future receiver designs. Although the metals described in this experiment have been shown to withstand impacts of alumina particles 800°C for extended periods, further experiments will determine the extended life of other materials, including ceramics which can withstand even higher temperatures.

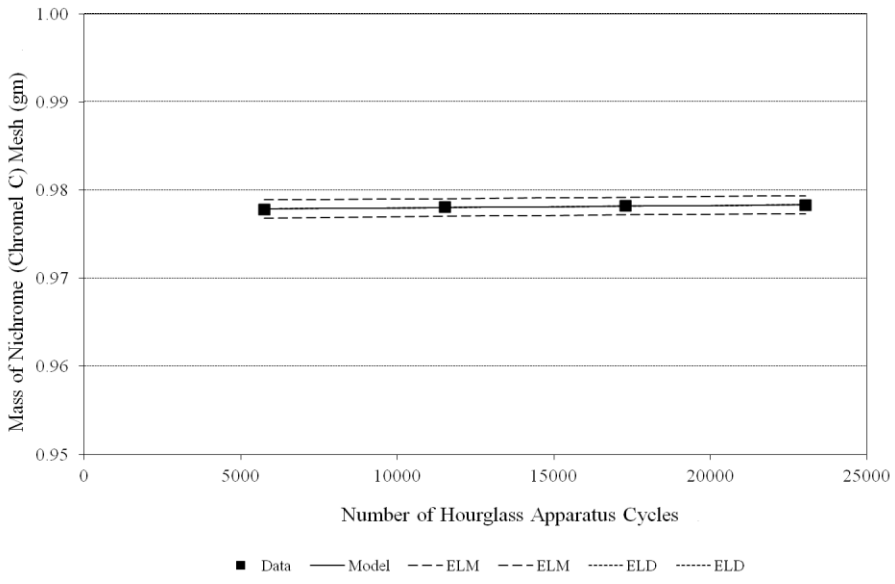

Figure 6.4 Graph of Chromel C Nickel-Chromium Alloy Mass vs. Cycles

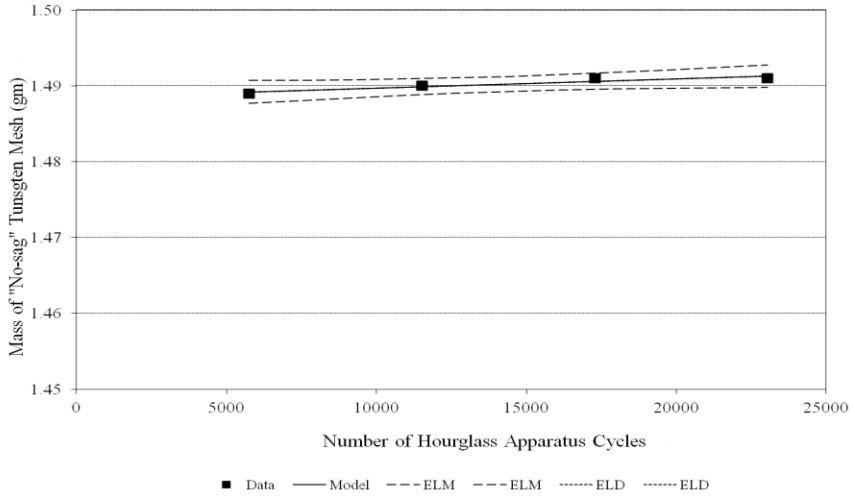

Figure 6.5 Graph of Non-Sag Tungsten Mass vs. Cycles

Oxidation Testing

After the testing in the hourglass apparatus, it became apparent that oxidation was an important factor in the mass of the samples, perhaps more than abrasion. To determine how much of the change in mass is due to oxidation, heating untested metal samples in a NETZSCH TGA/DSC was undertaken. Each sample is weighed before and after the heating process to determine the mass change due to oxidation. Appendix C describes the process in more detail.

The changes in mass for stainless steel 316, nickel chromium (Chromel C), and non-sag tungsten in the TGA/DSC were very similar to the change in mass in the hourglass apparatus. Stainless steel 316 increased 2.60% by mass in the hourglass, and 2.53% in the TGA/DSC. The nickel-chromium sample increased by 0.14% by mass in the hourglass, and 0.15% in the TGA/DSC. The non-sag tungsten was similar to the stainless steel and nickel-chromium samples. The increase in mass during the hourglass experiment for a non-sag tungsten sample was 0.27%, and increased by 0.28% in the TGA/DSC. These percentages demonstrate that the mass increase is due to oxidation, and that abrasion is negligible for these materials. However, it should be noted that the changes in mass for these samples are for similar sized wire strands used in the meshes. The size of the wire strands, the opening size of the meshes, the size of the particles, all of these are factors which must be taken into account.

CHAPTER 7

CONCLUSION

CSP is a viable and economical approach to commercializing solar power. However, common heat transfer mediums such as nitrate salts and steam impose limits on the commercial viability and efficiency of CSP systems. Nitrate salts corrode metals easily, are expensive, and are limited in their temperature range. The efficiency and cost effectiveness of steam are limited by the operating pressures. Replacing conventional heat transfer mediums with solid particulates is a method to reduce cost, increase the maximum temperature of the system, and have inherent thermal energy storage. All of these are advantages for CSP systems. When using particulates, several concerns arise, including the development of a receiver on the central tower. The receiver is a component that allows heat from solar radiation to be absorbed by a solid surface and transferred to the heat transfer medium. For nitrate salts and steam this surface is typically the pipes which carry the medium through the receiver. For solid particulates, a design which is being explored is a discrete structure particle heating receiver. The particulate is directly heated by the solar radiation by falling through the receiver. To slow down the particulate, discrete structure metal meshes are installed in the receiver. The particulate must flow through the meshes to pass through the receiver. The main challenge addressed in this thesis was whether or not various metals in the discrete structure PHR can withstand the repeated impact by high temperature particles and not undergo significant wear.

The experimental apparatus nicknamed the hourglass was designed and operated to test the durability of these materials. A fixed inventory of particles is allowed to fall through two samples of metal meshes fixed in place inside a SS316 pipe. The SS316 pipe and particles are

heated via two cartridge heaters attached to the pipe with endcaps to keep the particles inside the pipe. The pipe, cartridge heaters and endcaps, and isulation around the pipe are bolted to a rotating frame Attached to the rotating frame is a pulley system which is connected to a quarter turn pneumatic actuator. For a specified time and temperature the particulate is allowed to pass through the mesh samples. After the required time, the samples are cooled and are removed from the apparatus. The prior and post mass of the meshes are compared to show the change in mass in the experiment. From these mass changes the durability of the materials can be assessed.

Stainless steel 316, “no-sag” tungsten, and Chromel C nickel-chromium alloys were tested and show no sign of failure. There is oxidation of the surface but the meshes themselves are intact. The mass change of the meshes is positive because of oxidation of the materials. To test the effectiveness of the experiment, copper mesh was inserted into the apparatus and tested. The copper mesh failed. Significant scaling and abrasion caused the copper to weaken and fail under the high temperature impact conditions, although at what point during the 24 hour test the copper failed is not known. Stainless steel 316, “no-sag” tungsten, and Chromel C nickel-chromium are viable candidates for a PHR.

Since oxidation is observed on the surface of the materials, further long-term testing should be conducted on the mesh materials. Oxidation can cause scaling, which when impacted by falling particulate can cause the oxidation layer to chip away and reveal a new surface to be worn away. Or, if the scaling is not in action, then the oxidation layer can further serve as a barrier to protect the mesh.

APPENDIX A

ID50-K FOUNDRY PARTICULATE

Table A.1 Chemical Composition of ID50-K Particulate

Compound	Weight %
Al_2O_3	75.0
SiO_2	11.0
TiO_2	3.0
Fe_2O_3	9.0

Table A.2 Thermophysical Properties

ASG	3.23
GFN	40
Loose Bed Density (lbs/ft^3)	113
Packed Bed Density (lbs/ft^3)	125
Thermal Expansion (%LC)	0.708
Coefficient of Expansion (1E-6 in/in-°C)	6.62
Thermal Conductivity (W/m-°C)	0.70
Heat Capacity (cal/g-°C)	0.291
Thermal Diffusivity (cm^2/s)	0.0029
Heat Diffusivity 10^6(W^{2}s)/(m^4-°C^2)	1.708

Table A.3 Mineralogy (%) of ID50-K

Mullite	52
Corundum	48
Beta Cristobalite	0
Amorphous	0
Quartz Silica	0

Average Particle Diameter: 0.283 mm

APPENDIX B

SIFTING

The particulate in Appendix A is first sifted before being used in the experimental apparatus. This is to ensure that the particles are uniform in size and will not obstruct the mesh openings. The sifting device used is a Laboratory Test Sieve Vibrator built by the Derrick Mfg. Co. It is a Model 150, 25-60 cycle, 1/10 H.P., 0-6000 rpm sifter. In this experiment, 4200 RPM (70 Hz) was used. It was found by experimentation.

The sieves in the sifter are arranged top to bottom in order from widest mesh openings to smallest. Each sieve meets ASTM E-11 standards [15].

Figure B.1 Sifting Device with Stacked Sieves

Before each sifting, the sieves are removed and separated. Then compressed air is used to blow out trapped particles. Then the sieves are stacked again from largest opening area to smallest, top to bottom. The device is then turned on, and the rpm set to 4200. 10 minutes pass until the machine is turned off and the sieves are removed. The samples for the experiments are collected from below the U.S. 50 mesh and above the U.S. 70 mesh. This ensures that the particles placed into the apparatus are uniform.

APPENDIX C

TGA/DSC OXIDATION MEASUREMENTS

In order to determine the oxidation of the materials, a thermogravimetry analyzer-differential scanning calorimetery device (TGA/DSC) was used to heat metal samples up to 900°C. Figure C.1 shows a diagram of the instrument from NETZSCH.

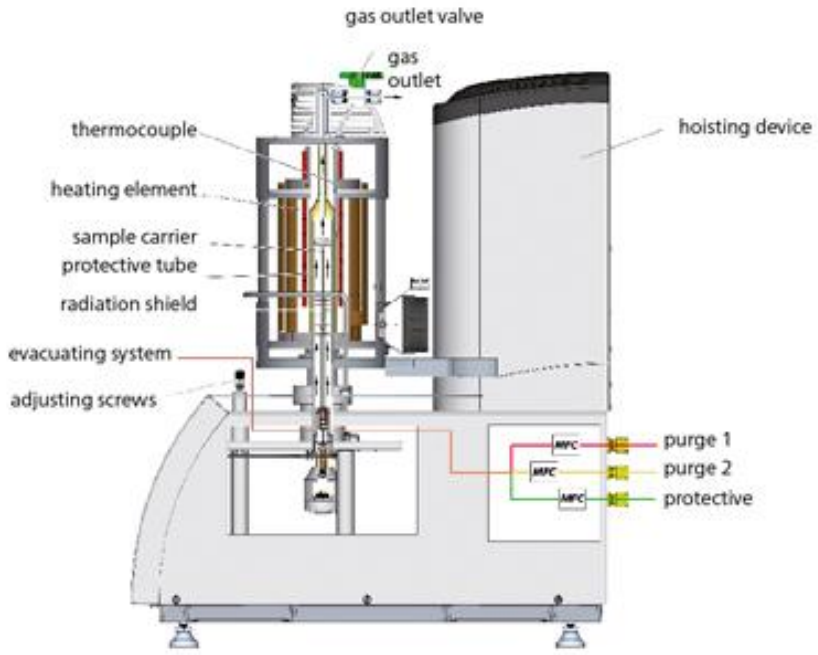

Figure C.1 Diagram of NETZSCH TGA/DSC

The material is weighed on a balance and then placed on the sample carrier. The sample carrier is placed inside the TGA/DSC and the housing is lowered. The desired gas flow rates and temperature profile are programmed. Then the testing starts.

After the sample is held at 900°C for 24 hours, or until the mass has reached a constant value, the sample is removed and weighed again. The change in mass the mass which has been oxidized.

REFERENCES

[1] "Selection and Conceptual Design of an Advanced Thermal Energy Storage Subsystem for Commerical Scale (100 MW_e) Solar central Receiver Power Plant," Babcock and Wilcox, Barberton, OH, pusblished by Sandia National Laboratories, Livermore, SAND 80-8190, February 1981.

[2] Martín, J, and Vitko, J. Jr., "ASCUAS: A Solar Central Receiver Utilizing a Solid Thermal Carrier," Sandia National Labroatories, Livermore, SAND82-8203, January 1982.

[3] Hruby, J. M., "A Technical Feasibility Study of a Solid Particle Solar Central Receiver for High Temperature Applications," Sandia National Laboratories, Livermore, SAND86-8211, March 1986.

[4] Falcone, P. K., Noring, J. E., and Hruby, J. M., "Assessment of a Solid Particle Receiver for a High Tempeature Solar Central Receiver System," Sandia National Laboratories, SAND85-8208, February 1985.

[5] Burolla, V. P., Hruby, J. M., and Steele, B. R., "High Solar Thermal Energy Absorption with Solid Particles," Proceedings of the 19th Intersociety Energy Conversion Engineering Conference, Vol. 3, August 1984, pp. 1663-1668.

[6] LaJeunesse, C. A., "Performance and Design of a Solid Particle Cavity Receiver," Sandia National Laboratories, SAND85-8206, April 1985.

[7] Kennedy Van Suan Company, "Pneumatic Conveying Systems and Components," bulletin PCS 3/84.

[8] Green, H., Leboeuf, C., and Bohn, M., "Technical and Economic Evaluation of a Solid-Particle/Air Direct-Contact Heat Exchanger," Solar Energy Research Institute, TR-252-2663, February 1986.

[9] Ho, C. and Iverson, B., "Review of High-Temeprature Central Receiver Designs for Concentrating Solar Power," *Renewable and Sustainable Energy Reviews*, **29**, Elsevier Ltd., pp. 835-846, August 2013. www.elsevier.com/locate/rser.

[10] Marti, J., Roesle, M., and Steinfeld, A., "Experimental Determination of the Radiative Properties of Particle Suspensions for High-Temperature Solar Receiver Applications," available online DOI:10.1080/01457632.2013.825173, *Heat Transfer Engineering*, **3**, Vol. 35, Feb. 2014.

[11] Golob, M., Jeter, S., Abdel-Khalik, S. I., Sadowski, D., Al-Ansary, H., and El-Leathy, A., "Development and Design Prototype 300kW-Thermal High-Temperature Particle Heating Concentrator Solar power System Utilizing Thermal Energy Storage," *Proceedings of the ASME 2014 8th Intern. Conf. on Energy Sustainability*, ASME, June 2014.

[12] Liu, H., Sakamoto, M., Nomura, M., Ogi, K., "Abrasion Resistance of High Cr Cast Irons at an Elevated Temperature," *Wear*, **250**, 2001, pp. 71-75.

[13] Nguyen, C., Roop, R., Knott, R., Abdel-Khalik, S. I., Jeter, S., Al-Ansary, H, "Preliminary Investigation of Particle Flow Characteristics Within Particle Heating Receivers," *Early Career Technical Conference 2014 Proceedings*, Vol. 13, UAB School of Engineering, November 2014.

[14] Misra, A. and Finnie, I., "A Review of the Abrasive Wear of Metals," *J. of Eng. Materials and Tech.*, Vol. 104, April 1982, pp. 94-101.

[15] ASTM Standard E11, 2013, "Standard Specification for Woven Wire Test Sieve Cloth and Test Sieves," ASTM International, West Conshohocken, PA, 2013, DOI: 10.1520/E0011, www.astm.org.